



**HAL**  
open science

# Coupling Exponential to Linear Amplification for Endpoint Quantitative Analysis

Coline Kieffer, Yannick Rondelez, Guillaume Gines

► **To cite this version:**

Coline Kieffer, Yannick Rondelez, Guillaume Gines. Coupling Exponential to Linear Amplification for Endpoint Quantitative Analysis. *Advanced Science*, 2024, 11 (21), <10.1002/advs.202309386>. <hal-04731759>

**HAL Id: hal-04731759**

**<https://hal.science/hal-04731759v1>**

Submitted on 11 Oct 2024

HAL is a multi-disciplinary open access archive for the deposit and dissemination of scientific research documents, whether they are published or not. The documents may come from teaching and research institutions in France or abroad, or from public or private research centers.

L'archive ouverte pluridisciplinaire HAL, est destinée au dépôt et à la diffusion de documents scientifiques de niveau recherche, publiés ou non, émanant des établissements d'enseignement et de recherche français ou étrangers, des laboratoires publics ou privés.



Distributed under a Creative Commons CC BY 4.0 - Attribution - International License

# Coupling Exponential to Linear Amplification for Endpoint Quantitative Analysis

Coline Kieffer, Yannick Rondelez, and Guillaume Gines\*

Exponential DNA amplification techniques are fundamental in ultrasensitive molecular diagnostics. These systems offer a wide dynamic range, but the quantification requires real-time monitoring of the amplification reaction. Linear amplification schemes, despite their limited sensitivity, can achieve quantitative measurement from a single end-point readout, suitable for low-cost, point-of-care, or massive testing. Reconciling the sensitivity of exponential amplification with the simplicity of end-point readout would thus break through a major design dilemma and open a route to a new generation of massively scalable quantitative bioassays. Here a hybrid nucleic acid-based circuit design is introduced to compute a logarithmic function, therefore providing a wide dynamic range based on a single end-point measurement. CELIA (Coupling Exponential amplification reaction to LLinear Amplification) exploits a versatile biochemical circuit architecture to couple a tunable linear amplification stage – optionally embedding an inverter function – downstream of an exponential module in a one-pot format. Applied to the detection of microRNAs, CELIA provides a limit of detection in the femtomolar range and a dynamic range of six decades. This isothermal approach bypasses thermocyclers without compromising sensitivity, thereby opening the way to applications in various diagnostic assays, and providing a simplified, cost-efficient, and high throughput solution for quantitative nucleic acid analysis.

testing<sup>[3]</sup>), exponential rolling circle amplification (eRCA, that leverages processive and strand-displacing enzymes like Phi29 DNA polymerase)<sup>[4]</sup> or Exponential Amplification reaction (EXPAR, which can be easily connected to diverse input targets like DNA, RNA, protein or even small metabolites)<sup>[5]</sup> allow exponential process going from a few copies of a nucleic acid target, up to easily detectable concentrations – typically via an optical readout. Quantification measurements, however, rely on the real-time kinetic monitoring of the reaction to extract an amplification time (e.g. cycle threshold, Ct for qPCR), which is logarithmically related to the initial target concentration (Figure 1A). As such, these exponential assays offer an exceptional dynamic range (up to 8 decades).<sup>[6]</sup> Although a simpler, endpoint measurement is possible, it drastically reduces the dynamic range<sup>[7]</sup> and is generally only used to retrieve qualitative (yes/no) information,<sup>[8]</sup> essentially because the exponentially amplified signal quickly reaches saturation (Figure 1B).

By contrast, linear amplification schemes such as RCA<sup>[9,10]</sup> or strand displacement amplification (SDA)<sup>[11]</sup> authorize quantitative endpoint readout. However, owing

to the slow, linear accumulation of signal, these methods are much less sensitive than their exponential counterparts and provide a linear dynamic range (Figure 1C).

In this work, we design a modular DNA/enzyme-based reaction network that allows for quantitative endpoint measurement of nucleic acid targets while maintaining the sensitivity and wide dynamic range of an exponential strategy. The concept relies on Coupling an Exponential amplification reaction to LLinear Amplification stage with tunable gain (CELIA, Figure 1D).

## 1. Introduction

Exponential DNA amplification methods are a cornerstone of ultrasensitive molecular diagnostics. Although polymerase chain reaction (PCR) is the most emblematic illustration<sup>[1,2]</sup>, isothermal amplification schemes are rapidly expanding, offering promising alternatives. For example, loop-mediated isothermal amplification (LAMP, used notably for rapid SARS CoV-2

C. Kieffer, Y. Rondelez, G. Gines  
Laboratoire Gulliver  
UMR7083 CNRS/ESPCI Paris-PSL Research University  
10 rue Vauquelin, Paris 75005, France  
E-mail: [guillaume.gines@espci.fr](mailto:guillaume.gines@espci.fr)

 The ORCID identification number(s) for the author(s) of this article can be found under <https://doi.org/10.1002/advs.202309386>

© 2024 The Authors. Advanced Science published by Wiley-VCH GmbH. This is an open access article under the terms of the [Creative Commons Attribution](#) License, which permits use, distribution and reproduction in any medium, provided the original work is properly cited.

DOI: 10.1002/advs.202309386

## 2. Results and Discussion

We built on a previously reported EXPAR-like molecular switch based on the polymerase-exonuclease-nickase (PEN) toolbox,<sup>[12,13]</sup> which allows exponential signal strand amplification while mitigating nonspecific reactions<sup>[14]</sup>. The original circuit is assembled from three DNA templates: the amplification template (aT $\alpha$ ) is a dual-repeat sequence embedding a nicking recognition site, which encodes the exponential replication of a signal strand ( $\alpha$ ) upon polymerization/nicking cycle; the pseudo-

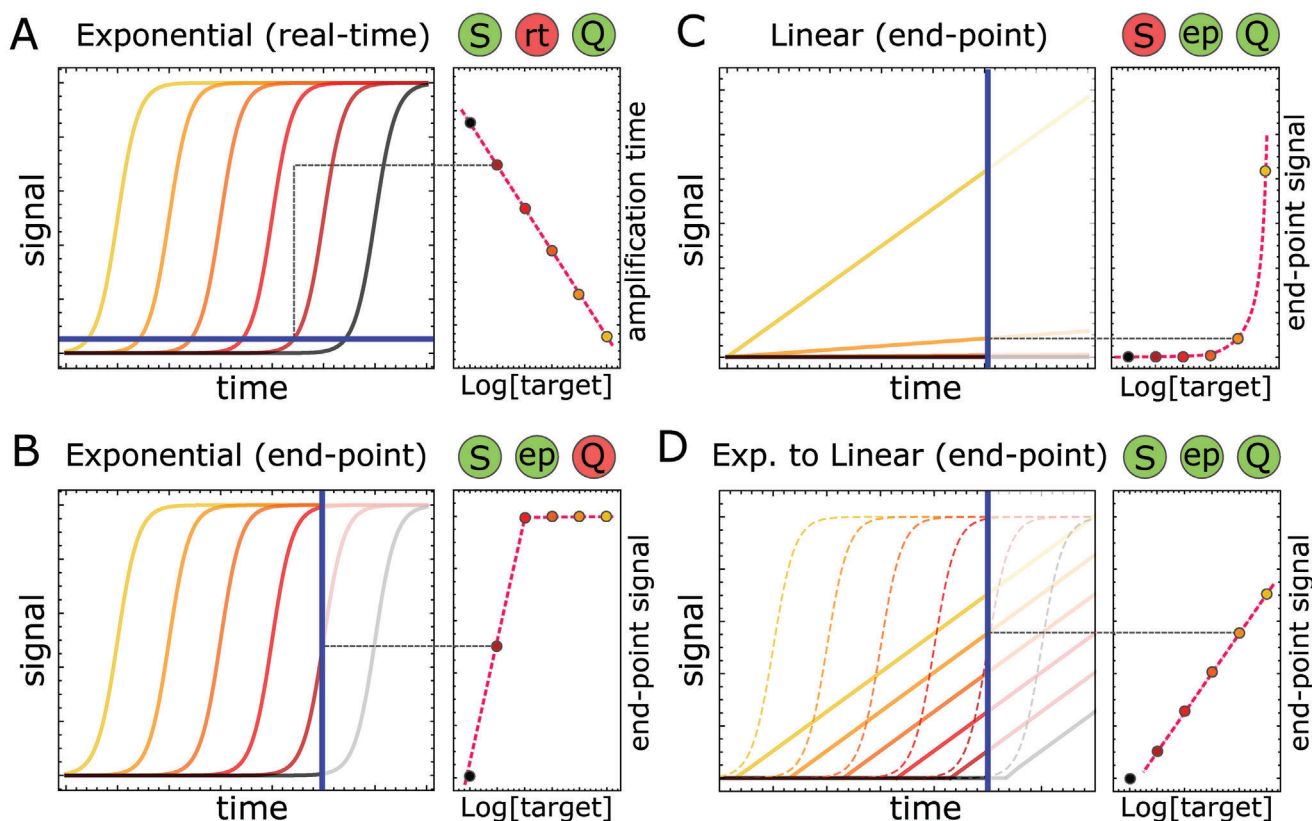


**Figure 1.** Comparison of the sensitivity (S), quantitativity (Q) and readout (real-time, rt or endpoint, ep) for various amplification schemes, applied to a serial dilution of a target. A) Exponential amplification enables highly sensitive target detection, but it requires the real-time monitoring of the amplification reaction to provide quantitative information. B) Exponential amplification reactions with endpoint analysis provide low-cost and fast readout, but the saturation of the signal occurs too rapidly to retrieve quantitative information, rendering it suitable only for qualitative analysis C) Linear amplification can be used for endpoint target quantification, however with a limited sensitivity due to the low amplification fold. D) The proposed CELIA approach combines the sensitivity of exponential amplification with the convenience and lower cost of endpoint readout afforded by linear amplification. This is achieved by conditionally implementing a linear amplification stage after the exponential amplifier stage. Horizontal and vertical blue lines correspond to the selected amplification signal threshold and endpoint time, respectively.

template ( $pT\alpha$ ) is made of the complementary sequence of  $\alpha$  to which is appended a short 5' polynucleotide sequence (e.g. pentathymidylate) that allows the deactivation of  $\alpha$  by polymerase extension;<sup>[14]</sup> the reporter template ( $rT\alpha$ ) is a hairpin-shape structure labeled with a fluorophore and a quencher, that is used to probe the presence of complementary  $\alpha$  strands. To implement a CELIA circuit, we connected this exponential amplification module to the linear production of a secondary signal strand ( $\omega$ ) by introducing two additional templates. The first one is a linear template ( $\alpha\omega$ ) that takes  $\alpha$  as input and creates  $\omega$  via polymerization/nicking cycles. The second one is a  $\omega$ -specific reporter template ( $rT\omega$ ) which reveals the accumulation of  $\omega$  in a second fluorescent channel.

We first tested the linear amplification module in isolation (see Figures S1–S5 (Supporting Information) for detailed reaction networks). We preloaded  $\alpha\omega$  with an excess of its input and monitored the signal generated by the red-fluorescent reporter  $rT\omega$  (Figure 2A). We indeed observed a linear response in time followed by a saturation phase when all  $rT\omega$  has reacted. Additionally, the response of this amplifier can be finely tuned in terms of i) the amplification gain, by varying the concentration of  $\alpha\omega$  (Figure 2E,F); ii) the signal saturation, which is di-

rectly proportional to the concentration of  $rT\omega$  (Figure 2D,F); iii) the linear amplification time window (before reaching saturation), which depends on the ratio between  $\alpha\omega$  and  $rT\omega$  (Figure 2C,F).

We next connected the linear amplification module downstream of an exponential amplification switch ( $\alpha T\alpha/pT\alpha/rT\alpha$ ) in such a way that the endpoint signal from the linear amplifier ( $rT\omega$  fluorescence) should be inversely correlated to the amplification time of the exponential switch ( $A_t$ , i.e. the time it takes for the  $rT\alpha$  fluorescence to rise above a given detectable value, Figure 3A and B). To check this correlation, we continuously modulated the  $A_t$  values between 10 and 1000 min by varying the initial concentration of  $\alpha$  initiator (the higher, the sooner the  $A_t$ ) and  $pT\alpha$  inhibitor (the higher, the later the  $A_t$ ,<sup>[14]</sup> Figure 3C left). The red ( $rT\omega$ ) fluorescence signal (Figure 3C right) reveals that the linear stage quasi-instantaneously kicks in following the  $\alpha$  amplification module, and rapidly reaches a linear regime (see also Figure S6B, Supporting Information). In this experiment, the  $\alpha\omega$  and  $rT\omega$  concentrations (2 and 200 nM respectively) were set so that the linear amplification window is larger than 1000 min, corresponding to the range of tested amplification times. We recorded the endpoint red ( $rT\omega$ ) fluorescence, which,

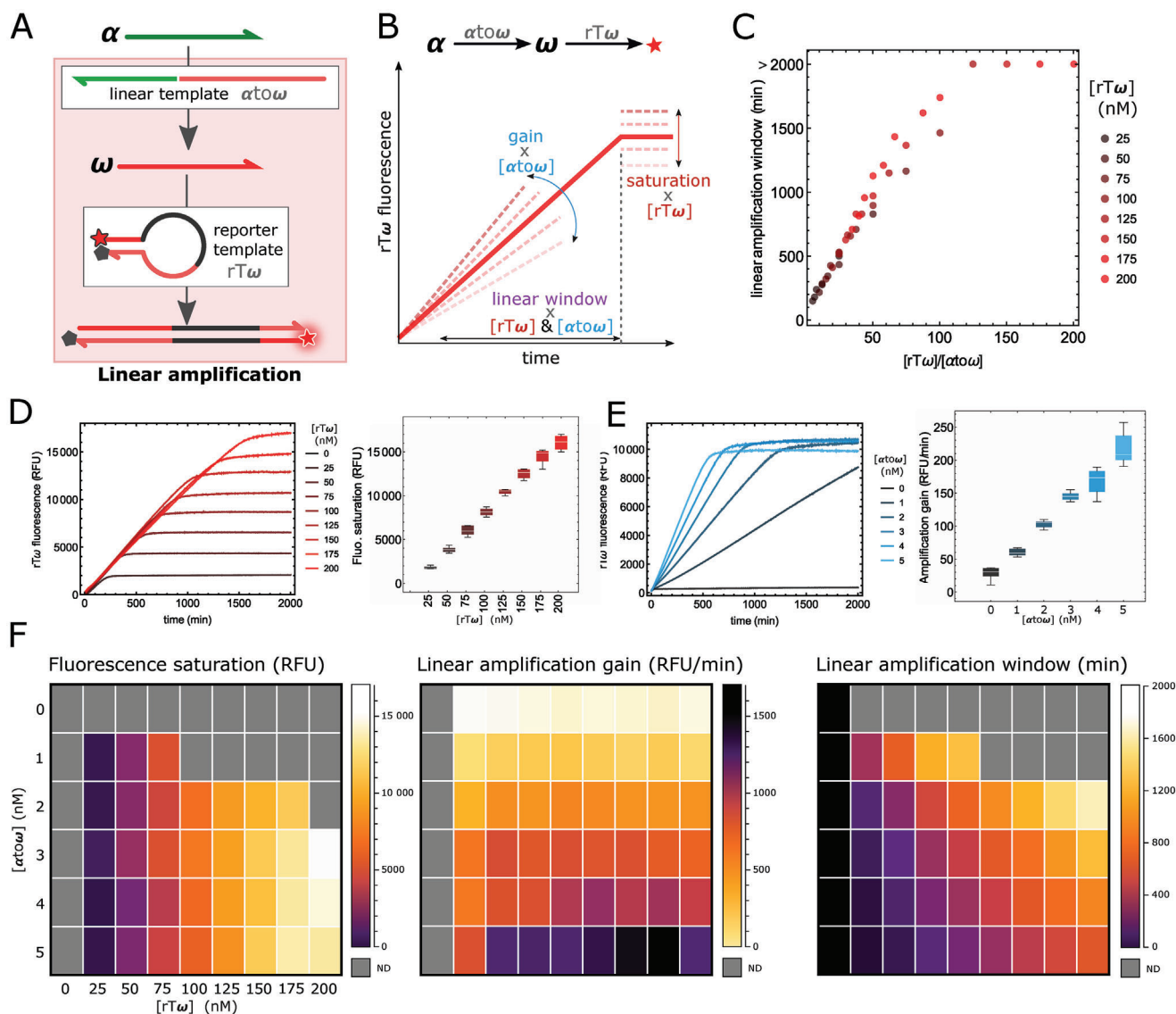


**Figure 2.** A linear amplification module with tunable response. A) The module is composed of the template  $\alpha t\omega$ , which linearly produces  $\omega$  once loaded with the  $\alpha$  input, and  $rT\omega$ , which generates a fluorescence signal once bound to  $\omega$ . B) The linear amplification is monitored in real-time for different concentrations of the two templates, allowing us to extract the amplification gain (related to the slope), the saturation level, and the linear response time window (i.e. the time it takes for the signal to reach saturation). C) Linear amplification window as a function of the ratio  $[rT\omega]/[\alpha t\omega]$ . D) Linear amplification curves for  $[\alpha t\omega] = 5$  nM and various  $[rT\omega]$ . The right plot corresponds to box and whisker chart of the  $rT\omega$  saturation level as a function of  $[rT\omega]$  for various  $[\alpha t\omega]$ . E) Linear amplification curves for  $[rT\omega] = 125$  nM and various  $[\alpha t\omega]$ . The right plot corresponds to box and whisker chart of the amplification gain as a function of  $[\alpha t\omega]$  for various  $[rT\omega]$ . F) Color-coded array plots of the fluorescence saturation (left), amplification gain (middle), and linear amplification window (right).

as expected, is negatively correlated to the At, with a coefficient of determination  $R^2 = 0.986$  (Figure 3D). The correlation can be improved by normalizing the  $rT\omega$  with the fluorescence at saturation (Figure S7, Supporting Information). This suggests that the slight deviation from the linear regression curve can be attributed in part to inter-well variations of the optical signal recorded by the real-time fluorescence scanner and would be mitigated with an appropriate fluorescent setup. Importantly, we verified that the linear amplification gain is consistent over time ( $1.15 \cdot 10^{-2} \pm 5.9 \cdot 10^{-4}$  RFU  $\text{min}^{-1}$ , CV  $\approx 5\%$ ) and independent from the exponential amplification time (Figure S6E, Supporting

Information). This is a crucial requirement for being able to use the endpoint  $rT\omega$  signal in quantitative biosensing applications.

Reversing the signal to obtain a positive correlation between the amplification time and the end-point  $rT\omega$  signal would enhance the modularity of the molecular circuit, enabling the implementation of logical operations (e.g., NOT gate), which are fundamental in building complex molecular programming systems.<sup>[15–17]</sup> The circuit architecture has been adjusted to encode such inverter function (Figure 4A): a converter template  $\beta t\omega$  constitutively produces  $\omega$  at a rate controlled by the concentration of  $\beta t\omega$  and its input  $\beta$  (Figure S8, Supporting

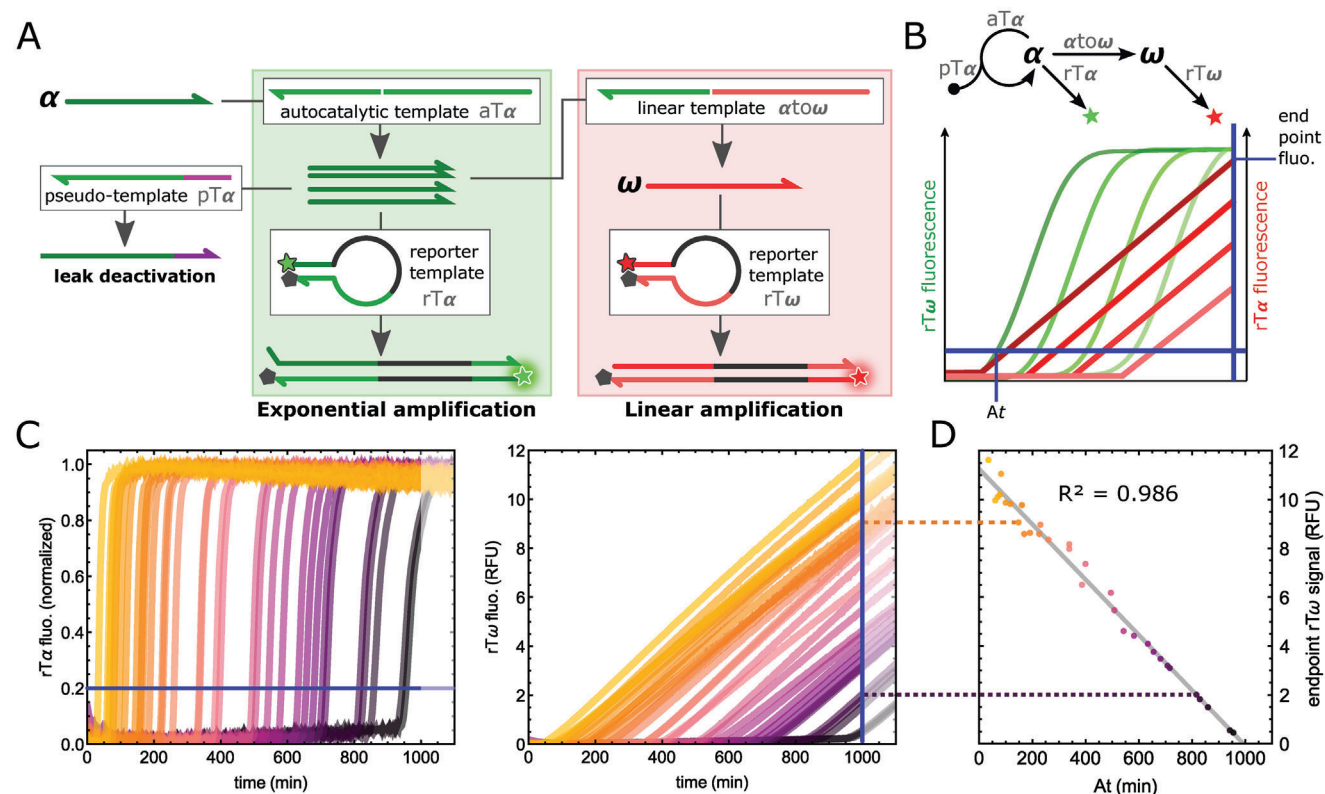


**Figure 3.** Negative linear correlation between the amplification time of the exponential module and the endpoint signal of the linear module. A) The linear module is connected downstream of an exponential amplification reaction, whose start time is controlled by the initial concentration of  $\alpha$  and  $pT\alpha$ . B) Both amplifications are monitored in parallel through the corresponding  $rT$  fluorescence, allowing the extraction of amplification times ( $rT\alpha$ ) and endpoint signals ( $rT\omega$ ). C) Time traces for the exponential (left) and linear amplification (right). Matching colors on the two plots correspond to the same sample (see also Figure S6, Supporting Information). The horizontal blue line materializes the signal threshold used to extract the amplification time ( $A_t$ ) in the exponential mode. The vertical blue line corresponds to the endpoint time in the linear amplification mode. D) Endpoint  $rT\omega$  ( $t = 1000$  min) as a function of the amplification time  $A_t$ .

Information). This linear amplification module hence generates a linear increase in  $rT\omega$  fluorescence from the beginning of the incubation. Once the exponential amplification of  $\alpha$  kicks in, it triggers the production of a  $\beta$  inhibitor under the form of a pseudo-template ( $pT\beta$ ) via the killer template  $\alpha k\beta$ <sup>[18]</sup> (which uses  $\alpha$  as input and produces  $pT\beta$  as output). Since  $\beta$  reversibly binds to  $\beta t\omega$  (Experimental Section, see the section on template design), it can hybridize to the newly produced  $pT\beta$ , and be extended by the DNA polymerase which releases an inactive form ( $\beta_i$ ). This stops the production of  $\omega$  and eventually makes the  $rT\omega$  signal plateau. Figure 4C shows the real-time amplification curves of  $\alpha$  (exponential) and  $\omega$  (linear). Like in the experiment shown in Figure 3, the  $\alpha$   $A_t$  is modulated by the  $pT\alpha$  inhibitor and the  $\alpha$  initiator concentration. As anticipated, the sooner the  $\alpha$  amplification, the lower the  $\omega$  plateau. The endpoint  $\omega$  signal is now positively correlated to the  $\alpha$  amplification time ( $R^2 = 0.985$ , Figure 4D). We noticed that the inhibition of the linear amplification occurs after a certain delay from the exponential amplification time, which is dependent on the linear amplification gain (i.e., the concentration of  $\beta$  and  $\beta t\omega$ , Figure S9, Supporting Information) and can be reduced by increasing the concentration of  $\alpha k\beta$ . However, increasing  $\alpha k\beta$  also aggravates the nonspecific production of  $pT\beta$  stemming from the leak of

the killer template (Figure S10, Supporting Information). Such a leak is responsible for the premature decrease of the  $\omega$  production rate and results in an underestimation of the endpoint  $\omega$  signal at high amplification time ( $> 250$  min for  $\alpha k\beta = 1$  nM).

The CELIA system was applied to the end-point quantification of microRNA (miRNA) biomarkers.<sup>[19]</sup> We connected the exponential-to-linear amplification circuit (with no inverter function) circuit downstream of a converter template (miRto $\alpha$ ) that transduces the presence of an input miRNA into the generation of  $\alpha$  strands (Figure 5A,B).<sup>[20]</sup> In this configuration, the higher the target miRNA concentration, the sooner the amplification, hence the higher the endpoint  $rT\omega$  fluorescence signal. The assay was calibrated for two miRNAs, let-7a and miR-203a, both of which have been demonstrated to be associated with cancer diseases.<sup>[21,22]</sup> The amplification mixture was spiked with a varying concentration of either of these miRNAs and the endpoint fluorescence of  $rT\omega$  ( $t = 1000$  min) is reported in Figure 5C. As expected, the endpoint signal is positively correlated to the miRNA concentration over 6 orders of magnitude, with a limit of detection (LoD, determined from the mean signal of the negative control plus 3 times the standard deviation) of 17 and 33 fM for let-7a and miR-203a, respectively. These values are in agreement with the LoD computed from the exponential amplification

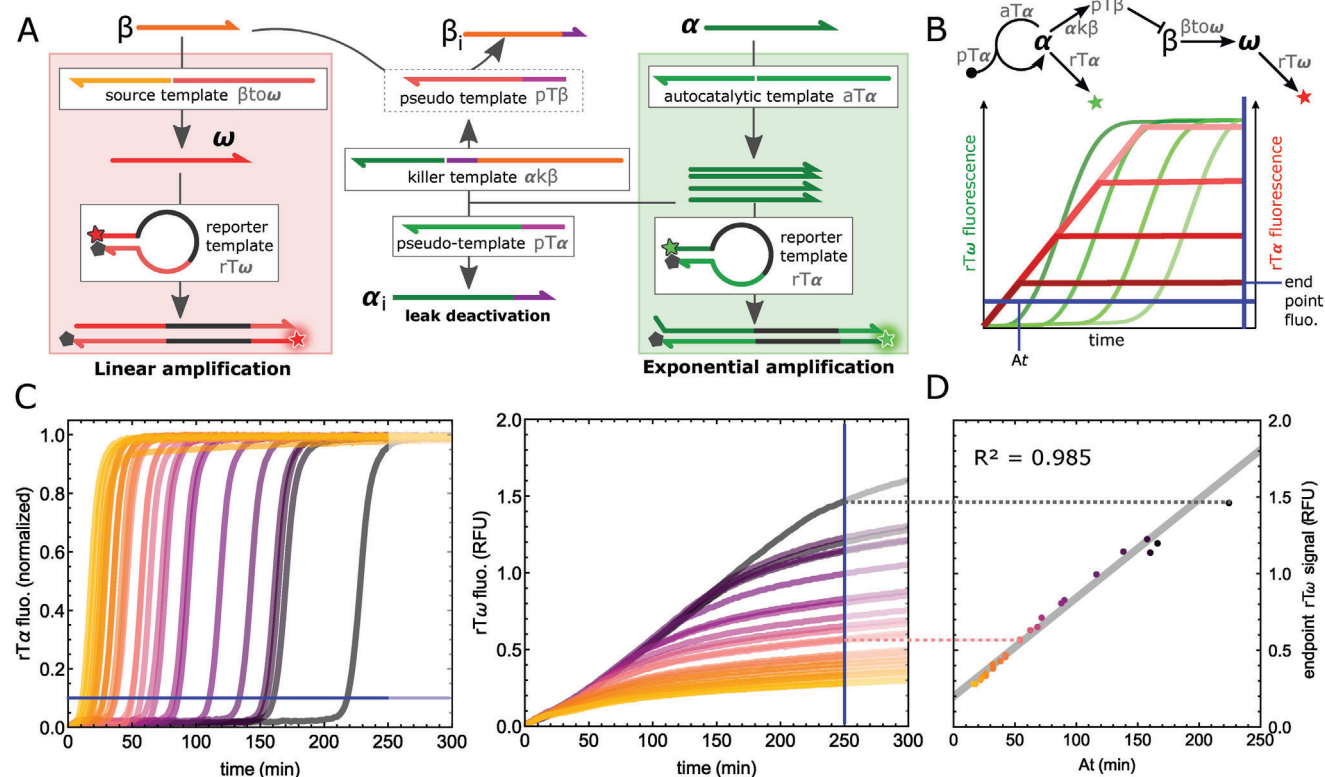


**Figure 4.** Inverter function. A) The circuit is composed of an exponential amplification module ( $aT\alpha$ ,  $pT\alpha$  and  $rT\alpha$ ) and a constitutive linear amplification module ( $\beta\tau\omega$ ,  $\beta$  and  $rT\omega$ ) interconnected by the killer template  $\alpha k\beta$ . Upon amplification of the  $\alpha$  signal,  $\alpha k\beta$  produces  $pT\beta$ , which in turn depletes the pool of  $\beta$  strand. This makes the linear amplification stop. As a result, the sooner the exponential amplification, the lower the endpoint linear amplification signal. B) Both amplifications are monitored in parallel through the corresponding  $rT$  fluorescence, allowing the extraction of amplification times ( $rT\alpha$ ) and endpoint signals ( $rT\omega$ ). C) Time traces for the exponential (left) and linear amplification (right). Matching colors on both graphs correspond to the same samples (see also Figure S11, Supporting Information). The horizontal blue line depicts the signal threshold for extracting the amplification time ( $At$ ) in the exponential mode and the vertical blue line corresponds to the endpoint chosen in the linear amplification mode. D) Endpoint  $rT\omega$  as a function of the amplification time. The data points are fitted with linear regression.

(28 and 16 fM, respectively, Figure S12, Supporting Information), demonstrating that the digital-to-analog signal conversion does not negatively impact the sensitivity. In addition, a simple linear amplification scheme (i.e. in the absence of any nonlinear signal amplification) displays a LoD of 8.5 pM (Figure S13, Supporting Information), supporting the gain of sensitivity brought by our exponential-to-linear amplification strategy, although optimized RT-qPCR assays displayed lower LoD (0.70 and 0.12 fM for let-7a and miR-203a, respectively (Figure S14, Supporting Information).

Leveraging miRNAs as biomarkers generally requires ultrasensitive detection, and thus real-time techniques.<sup>[23]</sup> The sample throughput is therefore limited by the immobilization of costly optical apparatus (e.g. 96-well qPCR machines) over the full duration of the assay. In the case of endpoint readout, on the contrary, many reactions can be incubated together offline, and then quickly analyzed in a sequential manner by a simple optical reader. To demonstrate that endpoint CELIA can indeed help mitigate the sample bottleneck in ultrasensitive diagnosis without compromising the quality of the measurement, we prepared 54 synthetic samples containing two clinically-relevant miRNAs (let-7a and miR-203a) at two different concentrations randomly taken from a uniform distribution on the interval 5 fM–100 pM in

logarithmic scale. Each miRNA of each sample was then individually assayed by using the cognate converter template in a CELIA reaction, and the endpoint  $rT\omega$  fluorescence was recorded. The experimental concentrations were then computed with reference to a calibration curve (Figure 5C). The two measured concentrations in each sample were very close to the expected pattern of spiked concentrations, with an average fold difference of  $2.3 \pm 1.4$  and  $2.1 \pm 1.9$  for let-7a and miR-203a, respectively (Figure 5D). Importantly, the real-time readout, performed in the same experiment, displays a similar, although slightly higher accuracy ( $1.8 \pm 1.3$  and  $1.5 \pm 0.7$  fold difference for let-7a and miR-203a, respectively (Figure S15, Supporting Information). However, we observed that when both miRNAs were present, the qPCR assay for miR-203a lacked specificity, resulting in a strong quantification bias (Figure S16, Supporting Information).

### 3. CELIA Circuit Design

In previously described isothermal exponential amplification schemes, real-time monitoring of the reaction is required to extract the amplification time, which linearly correlates with the log-concentration of the target (the higher the concentration, the sooner the amplification). Linear amplification schemes

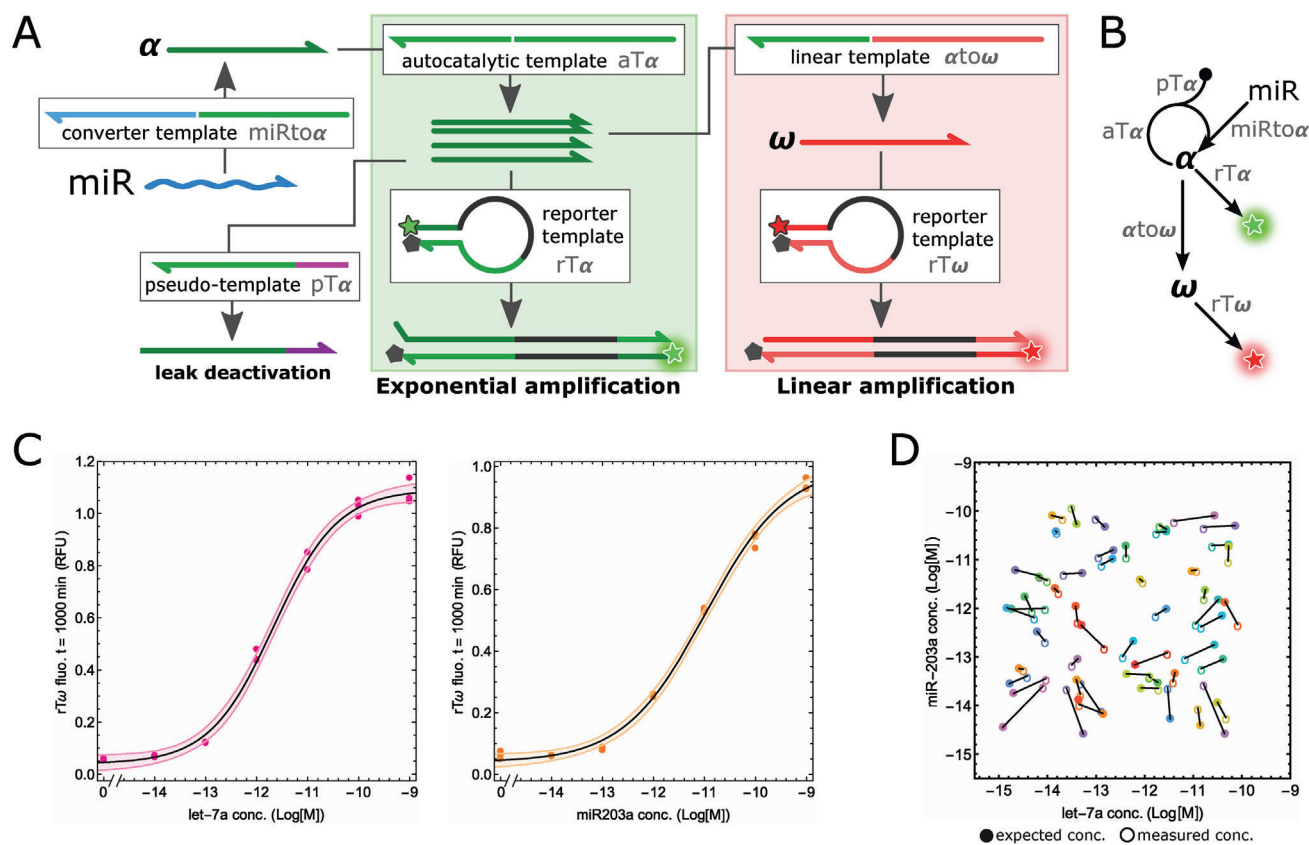


**Figure 5.** Endpoint readout applied to miRNA detection. A) Schematic of the miRNA endpoint sensing circuit. A miRNA converter template (miRto $\alpha$ ) is connected upstream to the exponential bistable module. B) Simplified scheme of the circuit architecture. C) Calibration curve for triplicated samples containing various concentration of let-7a (left) and miR-203a (right). The data points are fitted with a simple sigmoidal curve (black curve). The shaded area corresponds to the 90% confidence interval over the fitted parameters. D) Analysis of synthetic samples spiked with random concentrations of let-7a and miR-203a (from  $10^{-14}$  M to  $10^{-10}$  M).

offer the advantage of simpler, endpoint readout, at the cost of a lower sensitivity. For instance, the linear signal amplification provided by the collateral activity of CRISPR/Cas systems (e.g. Cas12a or Cas13a) has recently attracted considerable attention in diagnostics.<sup>[24–26]</sup> However, CRISPR detection schemes are often combined with a target pre-amplification step to increase their sensitivity to clinically-relevant levels.<sup>[27–29]</sup> In this work, we described a 1-step DNA/enzyme-based amplification circuit that converts the digital mode of a saturable exponential amplification to an analog regime through an additional linear amplification layer. The linear module gradually releases a fluorescent signal, thereby allowing ultrasensitive and wide dynamic range measurement via a single endpoint record. We demonstrated that the gain, tunable by simply varying the concentration of one template, is constant over time and does not depend on the amplification time, which indicates the robustness of the circuit and enzymes to experimental conditions. This constant gain is essential to preserve the quantitative nature of the real-time assay and to translate it to a simpler endpoint readout.

In addition, we provided the circuit with an inverter function that allows to reverse the correlation between amplification time and end-point signal. Such a feature would be of interest to transpose the assay to a simple and cost-efficient visual

readout (e.g. lateral flow assay or other colorimetric formats) for which a positive correlation facilitates the interpretability and intuitive understanding of the results. In the context of DNA computing, and more widely synthetic biology, such inverter (or NOT gate), where the input molecule induces a repression of the output molecule, is an essential component of – synthetic – gene regulatory networks, which can implement a wide range of dynamics.<sup>[30,31]</sup> We envision in the future the implementation of the presented circuit for neuromorphic molecular computing, which requires analog input integration and both positive and negative correlations.<sup>[17,32–35]</sup>

Our strategy of combining exponential and linear amplification modules to produce logarithmic responses in the concentration – not time – domain is in fact a general strategy that has already been proposed in other contexts.<sup>[36]</sup> Sanchez *et al.* reported an asymmetric implementation of PCR where the exponential replication of the double-stranded target sequence is followed by a linear production of single-stranded DNA from the primer in excess (LATE-PCR).<sup>[37]</sup> However, these efforts were developed in an attempt to improve real-time fluorescence reporting and were not leveraged for quantitative end-point protocols. To further support its usefulness and relevance in the field of ultrasensitive diagnostics, we tested the possibility of applying the exponential-

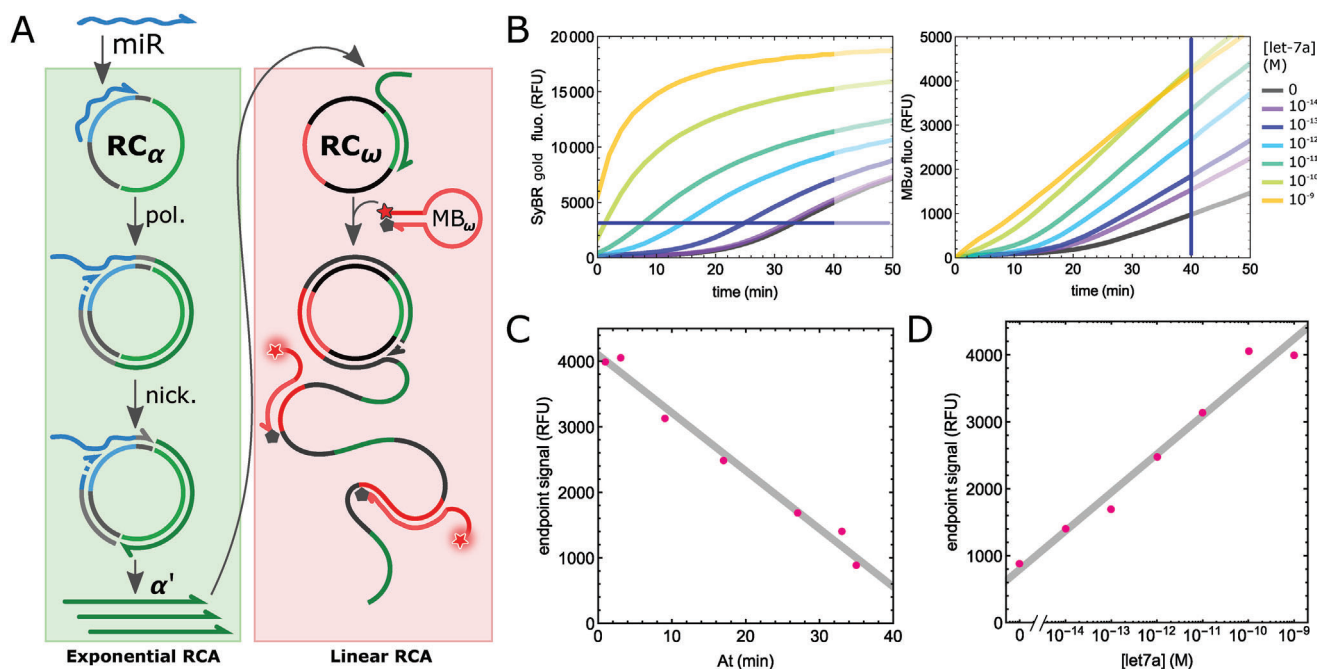


**Figure 6.** RCelia for sensitive and quantitative endpoint RCA. A) An exponential RCA is triggered by the miRNA target (let-7a). The nicking of the RCA product generates short DNA fragments that are used to load other circular templates. The output  $\alpha'$  of the exponential RCA initiates a secondary linear RCA on the circular template  $RC_{\omega}$ . This RCA product hybridizes to a pro-fluorescent molecular beacon  $MB_{\omega}$  that reports the progress of the reaction. B) Time traces for various let-7a concentrations of the exponential amplification (left, monitored with a double strand specific dye SYBR green) and linear amplification (monitored via  $MB_{\omega}$  fluorescence). It can be noted that the RCelia exponential amplification efficacy as well as the linear amplification gain decrease as the amplification increases. However, the linear stage reaches constant velocity following a short acceleration phase. These observations suggest a decrease in the enzymatic activity of the nicking enzyme essential to the exponential replication of  $\alpha'$ , but not required in the linear phase. C) Endpoint  $MB_{\omega}$  fluorescence as a function of At. D) Endpoint signal as a function of the let-7a target concentration.

to-linear strategy to other isothermal amplification primitives, such as the rolling circle amplification (RCA) reaction. We thus assembled the RCelia scheme, in which a nickase-assisted exponential RCA reaction<sup>[38]</sup> is combined with a second linear-only RCA (Figure 6A). The exponential RCA is initialized by the target miRNA (let-7a) and produces a short linear output ( $\alpha'$ ) by DNA polymerization and nicking along the circular probe  $RC_{\alpha}$ .  $\alpha'$  initiates the linear RCA along the second circular probe ( $RC_{\omega}$ ). Similar to the presented DNA circuit, while  $\alpha'$  is exponentially amplified up to a saturating level (monitored with the double-strand specific dye SYBR Gold), the downstream reaction restores a signal linearly correlated to the logarithm of the miRNA concentration, enabling endpoint, quantitative measurement, with a limit of detection in the sub-picomolar range, constrained by the nonspecific initiation of the RCA reaction (Figure 6B–D).<sup>[39]</sup>

Such quantitative endpoint readout mode would significantly reduce the burden of optical instrument run time and improve sample throughput. For instance, a typical RT-qPCR assay for miRNA quantification, performed in a 96-well plate format, requires 2 h of real-time thermocycling machine, leading to a maximum of 1152 samples in 24 h without delay between assays. By switching to an endpoint readout, the incubation step can be performed at a large scale (e.g. in a low-cost incubator) while the optical instruments are only used for the post-incubation measurement. With a 2 min turnover between measurements, the throughput can be increased by a factor of 60, allowing the testing of close to 70 000 samples per day.

## 4. Experimental Section

**Materials:** High-performance liquid chromatography-purified oligonucleotides were purchased from Biomers or Eurofins and resuspended at 100  $\mu\text{M}$  in 1X Tris–EDTA at pH 7.5 for long-term storage. The enzymes Nb.BsmI, Nb.BbvCI, Nb.BssSI, Nt.BstNBI, BsmI, DNA polymerase Vent (exo-), BSA (200  $\mu\text{g}\cdot\text{mL}^{-1}$ ) and dNTPs were obtained from New England Biolabs (NEB). A tenfold dilution of Nt.BstNBI was prepared in Diluent A supplemented 0.1% (v/v) Triton X100, and stored as the other enzymes at  $-20^{\circ}\text{C}$ . The CirLigase ssDNA was received from Biosearch Technologies. Phi29 DNA polymerase, Phi29 DNA polymerase reaction buffer 10X, DTT and SYBR Gold Nucleic Acid Gel Stain 10 000X were purchased from ThermoFisher. Thermus thermophilus RecJ exonuclease was produced in-house by following a previously published protocol<sup>[40]</sup> and was diluted by 140 in Diluent A (NEB) supplemented 0.1% (v/v) Triton X100 (Merck). Sodium chloride, potassium chloride, magnesium sulfate, ammonium sulfate, Trizma hydrochloride, nectropsin, and syneronic F104 were purchased from Merck (Sigma–Aldrich). All solutions were prepared using ultrapure water from a Millipore Milli-Q water purification system. Ligation and digestion reactions for RCA experiments were performed in an Eppendorf ThermoMixer C. All reactions presented in this paper were monitored with a CFX96 Touch Real-Time PCR machine (Bio-Rad) and the results were analyzed with Mathematica software (Wolfram).

**PEN-DNA Template Design:** Templates were designed according to the rules described elsewhere.<sup>[13,18,41]</sup> Template sequences  $\alpha$ ,  $pT\alpha$ ,  $\alpha\tau\omega$ ,  $\beta\tau\omega$ ,  $\alpha\kappa\beta$ , and  $rT\omega$  were protected against the 5'  $\rightarrow$  3' exonuclease activity of ttRecJ by the addition of three or four 5' phosphorothioate backbone modifications. Templates  $cT\alpha$ ,  $aT\alpha$ ,  $pT\alpha$ ,  $\alpha\tau\omega$ ,  $\beta\tau\omega$ , and  $\alpha\kappa\beta$  were blocked to prevent unwanted polymerization by the addition of a 3' phosphate moiety. The  $\alpha$  input binding site of  $aT\alpha$  was shortened by 2 bases to

hybridize only to the last 10 bases of the  $\alpha$  strand. This was to favor the deactivation by pT $\alpha$  of  $\alpha$  strands stemming from leaky reactions on aT $\alpha$  (resulting for instance from ab initio synthesis by the DNA polymerase).  $\alpha\omega$  ssDNA was designed to hybridize only the 93' bases of  $\alpha$  to minimize its competition with the autocatalytic template. The activation of  $\alpha\omega$  was made irreversible using a type IIS nicking site (Nt.BstNBI). In the case of the inverter function, the activation of the  $\beta\omega$  template for  $\omega$  production needs to be reversible to allow its inhibition by the killer template  $\alpha k\beta$ . To do so, the template contains a type IIP nicking site (Nb.BssSI) that is cleaved one base away from the 5' recognition sequence of the nickase. Cleavage of  $\beta\omega$  by Nb.BssSI releases an  $\omega$  with a 5' overhang corresponding to the recognition sequence, which does not affect the binding to and extension along rT $\omega$ . More importantly, the cleavage leaves a single additional 3' C on  $\beta$ , so that this modified input was still able to unbind from  $\beta\omega$  and be deactivated by the output of  $\alpha k\beta$ , hence permitting the blockage of  $\omega$  production. Note that the output of  $\alpha k\beta$  produces pT $\beta$ , a degradable pseudotemplate that can deactivate both  $\beta$  and its 3' C-extended version. See Table S1 (Supporting information) for a detailed list of the sequences used in this study and Figure S17 (Supporting information) for a schematic representation.

**PEN-DNA Reaction Assembly:** All reactions were assembled on ice. Ultrapure milliQ water and 4X reaction buffer (80 mM tris-HCl (pH 8.9), 40 mM (NH<sub>4</sub>)<sub>2</sub>SO<sub>4</sub>, 160 mM KCl, 40 mM MgSO<sub>4</sub>, 100  $\mu$ M each dNTP, 0.4% (w/v) Syneronic F108, 8  $\mu$ M netropsin) were mixed, followed by the addition of the templates, BSA (200  $\mu$ g.mL<sup>-1</sup>) and the enzymes (cf. Figure S18 (Supporting information) for exact sample composition). For miRNA detection, serial dilutions of a synthetic version of let-7a were performed on parafilm in Tris-EDTA 1X supplemented with 1 nM of pT $\alpha$  to minimize target carry-over. The dilution was executed using the pipet and mix mode of the electronic pipette Xplorer (Eppendorf), using a low binding DNA epDualfilter T.I.P.S. 1 – 20  $\mu$ L (Eppendorf, cat# 0030078500).

**Synthetic miRNA Samples:** Pairs of concentrations of let-7a and miR-203a were randomly selected in the logarithmic domain from the interval 10<sup>-14</sup>–10<sup>-12</sup> M. Sample assembly was performed on an automated liquid handling robot (I-DOT Deepwell, Dispensix) in 384-well plate (Bio-Rad), assisted by a custom-made script. Each sample was duplicated and spiked with either of the converter templates (let7ato $\alpha$  or 203ato $\alpha$ ). In addition, a calibration curve for each individual miRNA was realized with triplicate samples of a tenfold dilution of miRNA (from 10<sup>-9</sup> to 10<sup>-15</sup> M, including a no miRNA control). The standard data points were fitted with a sigmoid function:  $f(x) = L + H/(1 + b.e^{-k(x-x_0)})$ , where  $f(x)$  is the output (y-value) of the sigmoid function at input  $x$ ,  $L$  and  $H$  are respectively the lower and higher bound ( $L =$  lower and  $H + L =$  upper asymptote),  $k$  is the steepness of the curve and  $x_0$  the x-value at mid-point of the sigmoid.

**RCA Template Design:** RC $\alpha$  ssDNA template was designed to bind let-7a as an input. The RC $\alpha$  sequence contains two recognition sites for Nb.BbvCI such that each polymerization/nicking cycle releases one  $\alpha'$  strand and one secondary strand that were both released by polymerase-mediated strand displacement and bind free RC $\alpha$ . As a result, the target miRNA could trigger an initial exponential amplification of  $\alpha'$ . Subsequently,  $\alpha'$  partially binds RC $\omega$  and initiates the linear amplification stage. Note that RC $\omega$  templates did not contain any nicking site. The resulting polymerization upon RC $\omega$  generated a long ssDNA concatemer that bound and opened the stem of the molecular beacon (MB $\omega$ ). The loop of this hairpin-shaped molecular beacon has been designed to bind the output of the linear RCA template over 28 bases and to release fluorescence upon its hybridization at 37 °C. MB $\omega$  was conjugated with a Cyanine 5 fluorophore at the 5' extremity and with a BHQ-2 quencher at the 3' extremity. The stem composed of 8 bp and three 2'-O-methyl uracil was added to the 3' end to reinforce the stem structure at 37 °C.

**Circular Template Synthesis and Purification:** The ssDNA oligonucleotides were circularized with the CirLigase ssDNA (Biosearch Technologies). This enzyme is a thermostable ATP-dependent ligase that catalyzes the intramolecular ligation of ssDNA templates having 5'-phosphate and 3'-hydroxyl group at their extremities. The ligation reaction was performed in 1X Ligase reaction buffer from the provider, 50  $\mu$ M ATP, 2.5 mM MnCl<sub>2</sub>, 100 units CirLigase ssDNA, 1  $\mu$ M ssDNA template and supplemented with nuclease-free water to adjust the volume to 10  $\mu$ L.

The ligation reaction mixture was finally heated at 60&nbsp;°C for 2 h. The ligated products were subsequently treated with exonuclease I to remove unligated linear templates in 1X rCutSmart Buffer (NEB), 2 U. $\mu$ L<sup>-1</sup> of Thermolabile exonuclease I and 500 nM of ligated products. The digestion was pursued for 2 h at 37°C and the Exo I was finally deactivated at 80°C for 10 min. Samples were finally heated at 95°C for 10 min to unfold possible secondary structures of circular ssDNA templates, which were quantified by fluorometry using the Qubit 4 nucleic acid quantification (Invitrogen).

**RCA Reaction:** All reactions were assembled on ice. Ultrapure milliQ water and 10X Phi29 DNA polymerase reaction buffer (330 mM Tris-acetate (pH 7.9 at 37°C), 100 mM Mg-acetate, 660 mM K-acetate, 1% (v/v) Tween 20, 10 mM DTT) were mixed, followed by the addition of the two circular templates, 1 mM dNTPs, BSA (600  $\mu$ g.mL<sup>-1</sup>), 1.25X SYBR Gold and the necessary enzymes (cf. Figure S18 (Supporting Information) for exact sample composition). Samples were finally heated at 37°C to perform the exponential-to-linear reaction. The miRNA dilution protocol was identical to the PEN-DNA reaction described above.

**RT-qPCR Two-Step Procedure:** All reactions were assembled on ice. Target dilutions were performed on parafilm for the PEN-DNA reaction assembly section. The RT step was prepared by using the TaqMan MicroRNA Reverse Transcription Kit (cat #4366596, lot n°2888473) supplemented with the TaqMan microRNA assay for let-7a and miR-203a (cat #4427975). The qPCR step was performed with the TaqMan Universal Master Mix II, no UNG (cat #4440043, lot n°2768394) from ThermoFisher and with the PCR primers provided in the TaqMan microRNA assays. The entire RT-qPCR procedure was executed by following the protocol recommended by the provider. PCR thermocycling was performed in a CFX96 Touch Real-Time PCR machine (Bio-Rad) and the results were analyzed with Mathematica software (Wolfram).

## Supporting Information

Supporting Information is available from the Wiley Online Library or from the author.

## Acknowledgements

The authors thank the European Research Council for financial support (ERC Starting Grant MoP MiP, #949493).

## Conflict of Interest

The authors declare no conflict of interest.

## Data Availability Statement

The data that support the findings of this study are available from the corresponding author upon reasonable request.

## Keywords

CELIA, DNA circuits, DNA nanotechnology, endpoint readout, isothermal amplification, microRNAs, nucleic acid amplification

Received: December 3, 2023  
Revised: March 26, 2024  
Published online: April 9, 2024

[1] H. Zhu, H. Zhang, Y. Xu, S. Laššáková, M. Korabečná, P. Neužil, *BioTechniques*. **2020**, 69, 317.

- [2] M. Li, F. Yin, L. Song, X. Mao, F. Li, C. Fan, X. Zuo, Q. Xia, *Chem. Rev.* **2021**, *121*, 10469.
- [3] V. L. Dao Thi, K. Herbst, K. Boerner, M. Meurer, L. P. Kremer, D. Kirrmaier, A. Freistaedter, D. Papagiannidis, C. Galmozzi, M. L. Stanifer, S. Boulant, S. Klein, P. Chlanda, D. Khalid, I. Barreto Miranda, P. Schnitzler, H.-G. Kräusslich, M. Knop, S. Anders, *Sci. Transl. Med.* **2020**, *12*, 7075.
- [4] L. Xu, J. Duan, J. Chen, S. Ding, W. Cheng, *Anal. Chim. Acta.* **2021**, *1148*, 238187.
- [5] M. S. Reid, X. C. Le, H. Zhang, *Angew. Chem., Int. Ed.* **2018**, *57*, 11856.
- [6] C. Shi, Q. Liu, C. Ma, W. Zhong, *Anal. Chem.* **2014**, *86*, 336.
- [7] T. D. Schmittgen, B. A. Zakrajsek, A. G. Mills, V. Gorn, M. J. Singer, M. W. Reed, *Anal. Biochem.* **2000**, *285*, 194.
- [8] J. V. J. Silva Júnior, I. Merchioratto, P. S. B. de Oliveira, T. R. Rocha Lopes, P. C. Brites, E. M. de Oliveira, R. Weiblen, E. F. Flores, *J. Virol. Methods.* **2021**, *288*, 114007.
- [9] Q. Yao, Y. Wang, J. Wang, S. Chen, H. Liu, Z. Jiang, X. Zhang, S.-M. Liu, Q. Yuan, X. Zhou, *ACS Nano.* **2018**, *12*, 6777.
- [10] C. Li, H. Chen, J. Hu, C. Zhang, *Chem. Sci.* **2020**, *11*, 5724.
- [11] A. Joneja, X. Huang, *Anal. Biochem.* **2011**, *414*, 58.
- [12] K. Montagne, R. Plasson, Y. Sakai, T. Fujii, Y. Rondelez, *Mol. Syst. Biol.* **2011**, *7*, 466.
- [13] A. Baccouche, K. Montagne, A. Padirac, T. Fujii, Y. Rondelez, *Methods.* **2014**, *67*, 234.
- [14] K. Montagne, G. Gines, T. Fujii, Y. Rondelez, *Nat. Commun.* **2016**, *7*, 13474.
- [15] L. Qian, E. Winfree, *Science.* **2011**, *332*, 1196.
- [16] F. Wang, H. Lv, Q. Li, J. Li, X. Zhang, J. Shi, L. Wang, C. Fan, *Nat. Commun.* **2020**, *11*, 1.
- [17] C. Kieffer, A. J. Genot, Y. Rondelez, G. Gines, *Advanced Biology.* **2023**, *7*, 2200203.
- [18] Y. Rondelez, G. Gines, *ACS Sens.* **2020**, *5*, 2430.
- [19] J. Wang, J. Chen, S. Sen, *J. Cell. Physiol.* **2016**, *231*, 25.
- [20] G. Gines, R. Menezes, K. Nara, A.-S. Kirstetter, V. Taly, Y. Rondelez, *Sci. Adv.* **2020**, *6*, 5952.
- [21] P. Biswal, A. Lalruatfela, S. K. Behera, S. Biswal, B. Mallick, *IUBMB Life.* **2024**, *76*, 108.
- [22] J. Balzeau, M. R. Menezes, S. Cao, J. P. Hagan, *Frontiers in Genetics.* **2017**, *8*.
- [23] G. Gines, R. Menezes, W. Xiao, Y. Rondelez, V. Taly, *Molecular Aspects of Medicine.* **2019**, *72*, 100832.
- [24] S. Gong, S. Zhang, F. Lu, W. Pan, N. Li, B. Tang, *Anal. Chem.* **2021**, *93*, 11899.
- [25] Q. A. Phan, L. B. Truong, D. Medina-Cruz, C. Dincer, E. Mostafavi, *Biosens. Bioelectron.* **2022**, *197*, 113732.
- [26] M. M. Kaminski, O. O. Abudayyeh, J. S. Gootenberg, F. Zhang, J. J. Collins, *Nat. Biomed. Eng.* **2021**, *5*, 643.
- [27] J. S. Gootenberg, O. O. Abudayyeh, J. W. Lee, P. Essletzbichler, A. J. Dy, J. Joung, V. Verdine, N. Donghia, N. M. Daringer, C. A. Freije, C. Myhrvold, R. P. Bhattacharyya, J. Livny, A. Regev, E. V. Koonin, D. T. Hung, P. C. Sabeti, J. J. Collins, F. Zhang, *Science.* **2017**, *356*, 438.
- [28] C. Myhrvold, C. A. Freije, J. S. Gootenberg, O. O. Abudayyeh, H. C. Metsky, A. F. Durbin, M. J. Kellner, A. L. Tan, L. M. Paul, L. A. Parham, K. F. Garcia, K. G. Barnes, B. Chak, A. Mondini, M. L. Nogueira, S. Isern, S. F. Michael, I. Lorenzana, N. L. Yozwiak, B. L. MacInnis, I. Bosch, L. Gehrke, F. Zhang, P. C. Sabeti, *Science.* **2018**, *360*, 444.
- [29] J. S. Chen, E. Ma, L. B. Harrington, M. Da Costa, X. Tian, J. M. Palefsky, J. A. Doudna, *Science.* **2018**, *360*, 436.
- [30] H. Tas, L. Grozinger, R. Stoof, V. de Lorenzo, Á. Goñi-Moreno, *Nat. Commun.* **2021**, *12*, 355.
- [31] J. A. N. Brophy, C. A. Voigt, *Nat. Methods.* **2014**, *11*, 508.
- [32] S. Okumura, G. Gines, N. Lobato-Dauzier, A. Baccouche, R. Deteix, T. Fujii, Y. Rondelez, A. J. Genot, *Nature.* **2022**, *610*, 496.
- [33] K. M. Cherry, L. Qian, *Nature.* **2018**, *559*, 370.
- [34] R. Lopez, R. Wang, G. Seelig, *Nat. Chem.* **2018**, *10*, 746.
- [35] C. Zhang, Y. Zhao, X. Xu, R. Xu, H. Li, X. Teng, Y. Du, Y. Miao, H. Lin, D. Han, *Nat. Nanotechnol.* **2020**, *15*, 709.
- [36] R. Daniel, J. R. Rubens, R. Sarpeshkar, T. K. Lu, *Nature.* **2013**, *497*, 619.
- [37] J. A. Sanchez, K. E. Pierce, J. E. Rice, L. J. Wangh, *Proc. Natl. Acad. Sci. USA.* **2004**, *101*, 1933.
- [38] L. D. Smith, S. Nalla, C.-W. Kuo, M. Kohli, A. M. Smith, *Analyst.* **2022**, *147*, 2936.
- [39] V. K. Nair, C. Sharma, S. Ghosh, *ChemRxiv* **2022**, <https://doi.org/10.26434/chemrxiv-2022-mxtb3-v3>.
- [40] A. Yamagata, R. Masui, Y. Kakuta, S. Kuramitsu, K. Fukuyama, *Nucleic Acids Res.* **2001**, *29*, 4617.
- [41] Y. Rondelez, G. Gines, in *MicroRNA Detection and Target Identification: Methods and Protocols*. (Ed.: T. Dalmay), Springer US, New York, NY **2023**, pp. 89–102.